3D Cellular CoS$_{1.097}$/Nitrogen Doped Graphene Foam: A Durable and Self-supported Bifunctional Electrode for Overall Water Splitting

Hui Liang[1,†], Degang Jiang[1,†], Shuang Wei[1], Xueying Cao[1],Tao Chen[1], Bingbing Huo[1], Zhi Peng[2,*], Chenwei Li[1,*]and Jingquan Liu[1,*]

[1]College of Materials Science and Engineering, Institute for Graphene Applied Technology Innovation, Qingdao University, Qingdao 266071, China

[2]College of Materials Science and Engineering, Collaborative Innovation Centre for Marine Biomass Fibers, Materials and Textiles of Shandong Province, Qingdao University, Qingdao 266071, China

*Corresponding author. Prof. Dr. Zhi Peng; Dr. Chenwei Li; Prof. Dr. Jingquan Liu

E-Mail: pengzhi2001@163.com (Zhi Peng); lichenwei@qdu.edu.cn (Chenwei Li); jliu@qdu.edu.cn (Jingquan Liu)

[†]Hui Liang and Degang Jiang contribute equally to this work.

Experimental section

Electrochemical impedance spectroscopy (EIS)

EIS was performed on the materials under the OER operating conditions. A sinusoidal voltage with an amplitude of 5 mV and a scanning frequency ranging from 100 kHz to 10 mHz were applied to carry out the measurements. The EIS response for each material was then fitted with a simplified Randles equivalent circuit.

Effective electrode surface area (ECSA) calculation

In order to estimate the ECSA of the materials, cyclic voltammograms (CVs) of the synthesized materials in 1 M KOH were obtained in a potential window of 1.168 to 2.268 V vs. RHE for 20 cycles to activate them. The electrochemical double layer capacitance (Cdl) of each material at non-Faradaic overpotentials was probed using the CVs at different scan rates (20 mV s^{-1}, 40 mV s^{-1}, 60 mV s^{-1}, 80 mV s^{-1}and 100 mV s^{-1}). When the difference in current density (J) between the anodic and cathodic sweeps (Janodic - Jcathodic) at 1.218 V vs. RHE against the scan rate was plotted, a linear relationship between the two was obtained. The slope of the fitted line of the data points, which is twice the Cdl was then determined. The ECSA can then be estimated using the following equation, Eqn. S1:

$$ECSA= Cdl/Cs \qquad \text{Eqn. S1}$$

where Cs is the specific capacitance, whose value was reported to be 0.040 mF cm^{-2} in 1 M KOH.[S1]

Density function theory (DFT) method

All the density functional theory (DFT) calculations were performed using Vienna Ab-initio Simulation Package[S2, S3] (VASP) under the Projected Augmented Wave[S4] (PAW) method. The revised Perdew-Burke-Ernzerhof (RPBE) function was used to describe the exchange and correlation effect.[S5-S7] For all the geometry optimizations, the cutoff energy was set to be 450 eV. Spin-polarization calculations were included in all cases. The surface of $CoS_{1.097}$ was simulated to represent the catalytic interface. A $3\times3\times1$ Monkhorst-Pack grids[S8] was used to carry out the surface calculations on all the models. At least 15 Å vacuum layer was applied in z-direction of the slab models, preventing the vertical interactions between slabs.

The computational hydrogen electrode (CHE) model[S9] was used to calculate the free energies of HER and OER. For HER, it is a two-step process and involves only one reaction intermediate, the chemisorbed H atom. For the anodic OER, four steps involving three reaction intermediates are needed to generate oxygen gas. The free energy of these chemisorbed states is defined as (taking the H as an example):

$$\Delta G_{H^*} = \Delta E_H + \Delta E_{ZPE} - T\Delta S_H$$

Where, ΔE_H is the hydrogen binding energy, ΔE_{ZPE} is the zero point energy difference between adsorbed hydrogen and gaseous hydrogen, and $T\Delta S$ is the corresponding entropy difference between these two states. According to previous studies[S10], here we used a value of 0.24 eV to represent the correction of zero point energy and entropy of hydrogen state. The corrections of zero point energy and entropy of the OER intermediates can be found in the supporting information.
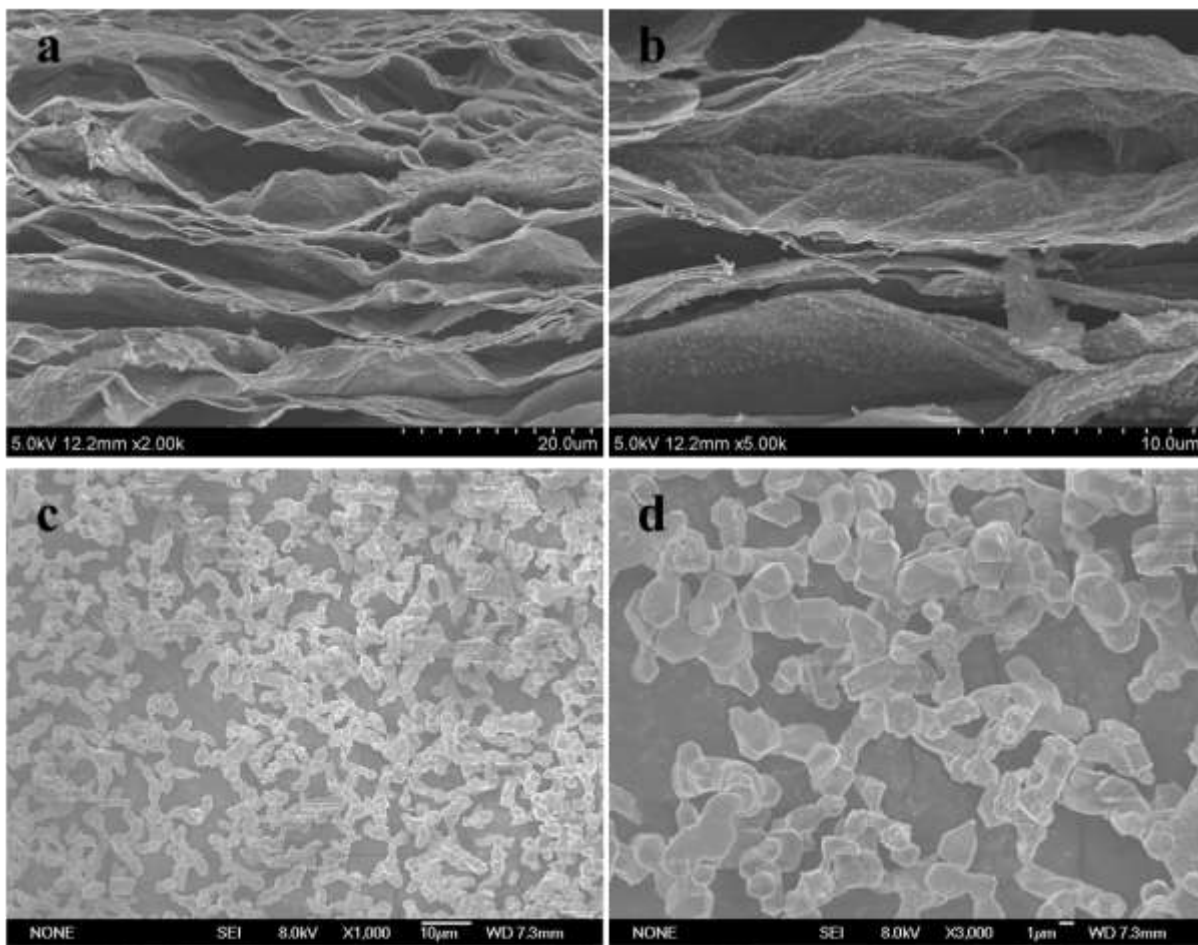
Fig. S1. (a, b) Cross-section SEM images of $CoS_{1.097}$/NGF-750. (c, d) SEM images of $CoS_{1.097}$ NPs.
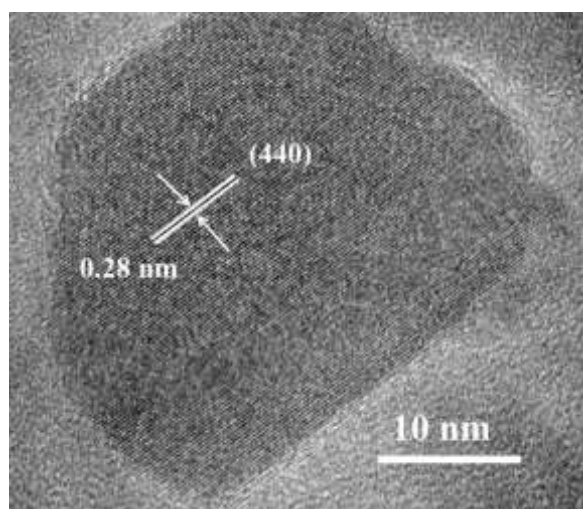
Fig. S2. HRTEM images of Co_4S_3/NGF.
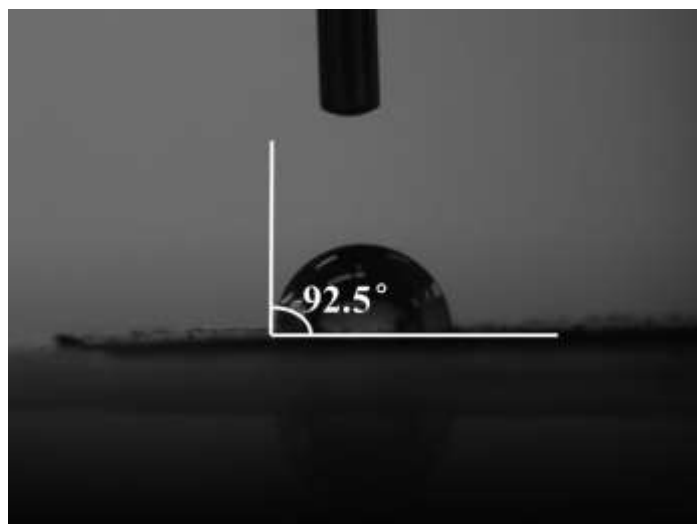
Fig. S3. The water contact angle measurement for GF-750.
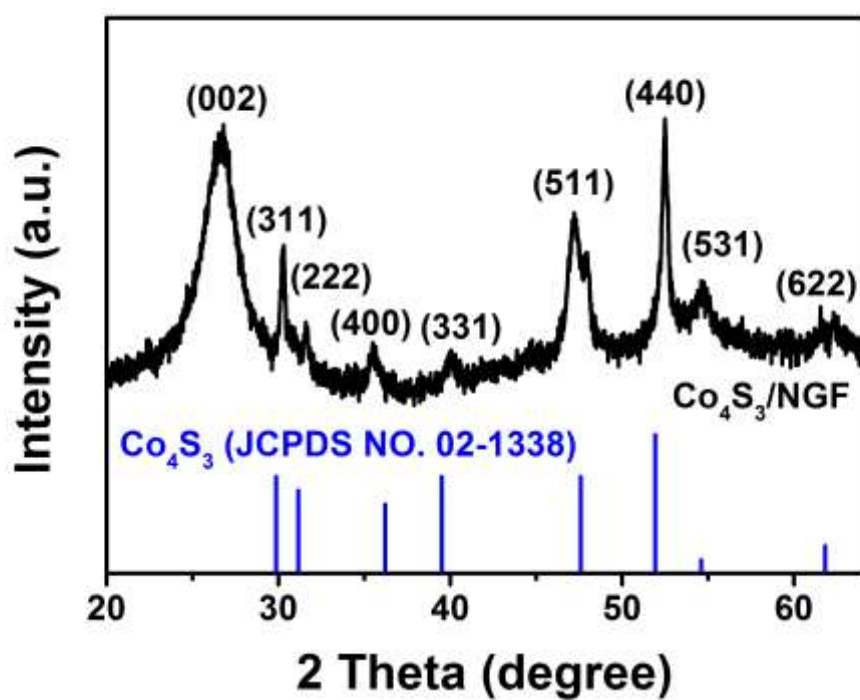
Fig. S4. XRD patterns of Co$_4$S$_3$/NGF.
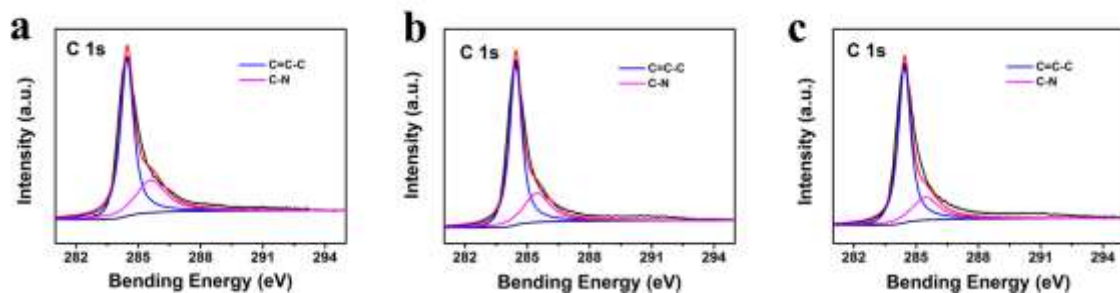
Fig. S5. The high-resolution XPS spectra for C 1s of (a) $CoS_{1.097}$/NGF-650, (b) $CoS_{1.097}$/NGF-850, and (c) $CoS_{1.097}$/NGF-950.
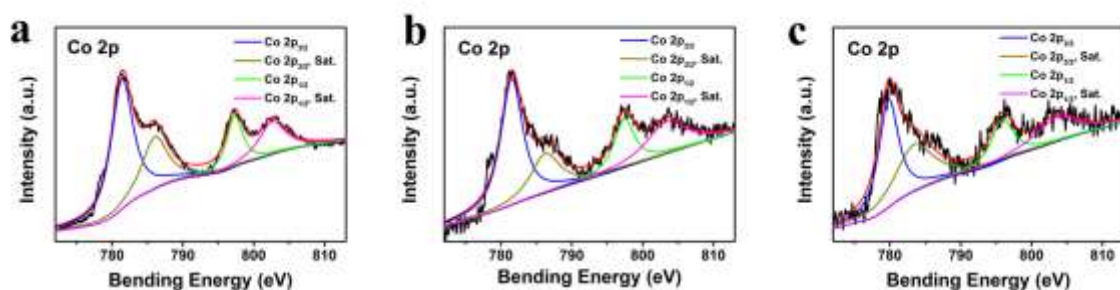
Fig. S6. The high-resolution XPS spectra for Co 2p of (a) $CoS_{1.097}$/NGF-650, (b) $CoS_{1.097}$/NGF-850, and (c) $CoS_{1.097}$/NGF-950.
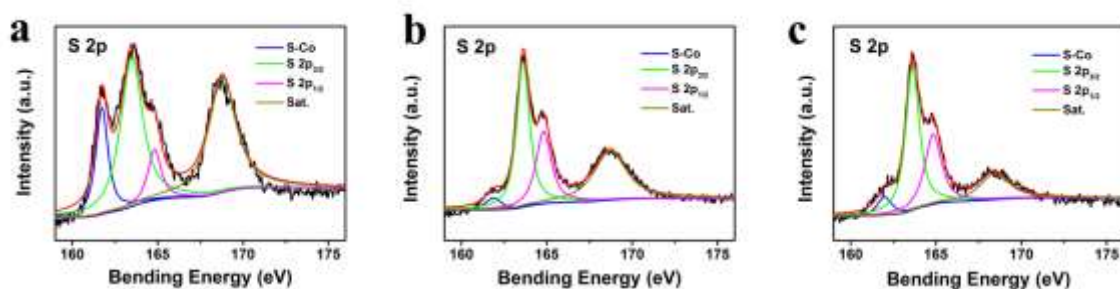
Fig. S7. The high-resolution XPS spectra for S 2p of (a) $CoS_{1.097}$/NGF-650, (b) $CoS_{1.097}$/NGF-850, and (c) $CoS_{1.097}$/NGF-950.
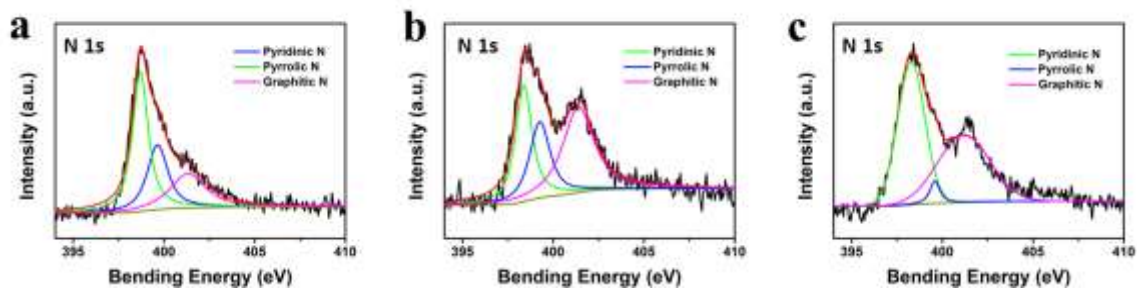
Fig. S8. The high-resolution XPS spectra for N 1s of (a) $CoS_{1.097}$/NGF-650, (b) $CoS_{1.097}$/NGF-850, and (c) $CoS_{1.097}$/NGF-950.
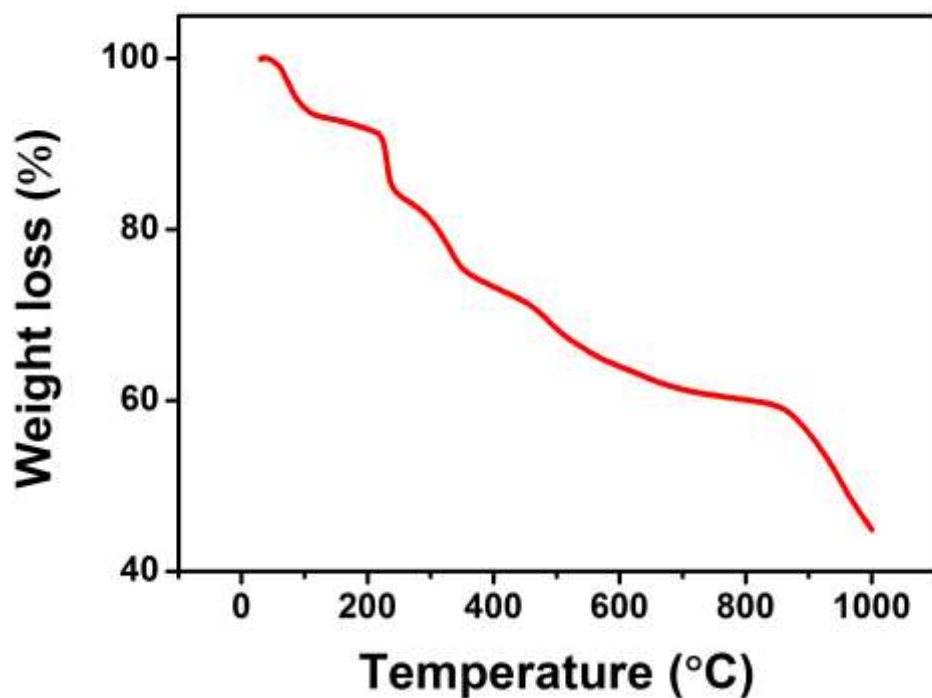
Fig. S9. Thermogravimetric analysis (TGA) curves of Co_4S_3/NGF in N_2 atmosphere from 30 °C to 1000 °C.
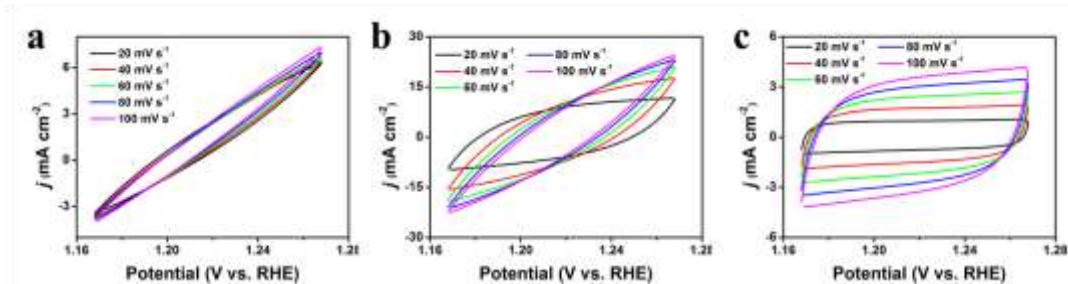
Fig. S10. Cyclic voltammograms (CVs) for $CoS_{1.097}$/NGF-(650, 850 and 950) at scan rates of 20, 40, 60, 80 and 100 mV s^{-1}, respectively.
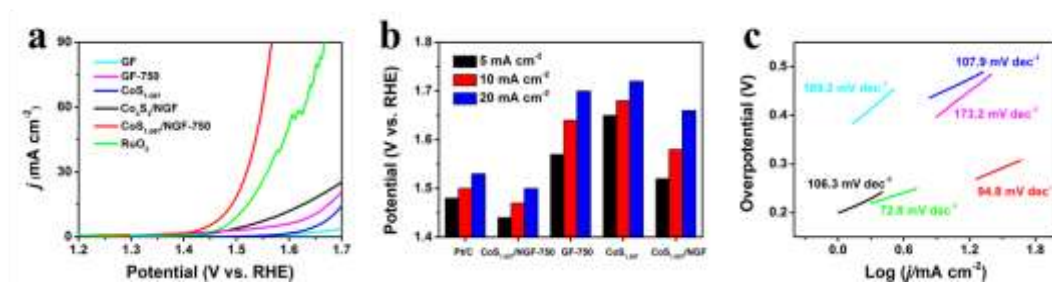
Fig. S11. Electrochemical OER properties of the electrocatalysts in 1 M KOH solution. (a) Polarization curves (iR-corrected) at a scan rate of 5 mV s^{-1}, (b) Potentials corresponding to different current densities (5, 10, 20 mA cm^{-2}) and (c) Tafel plots of GF, GF-750, $CoS_{1.097}$, Co_4S_3/NGF, $CoS_{1.097}$/NGF-750 and RuO_2.
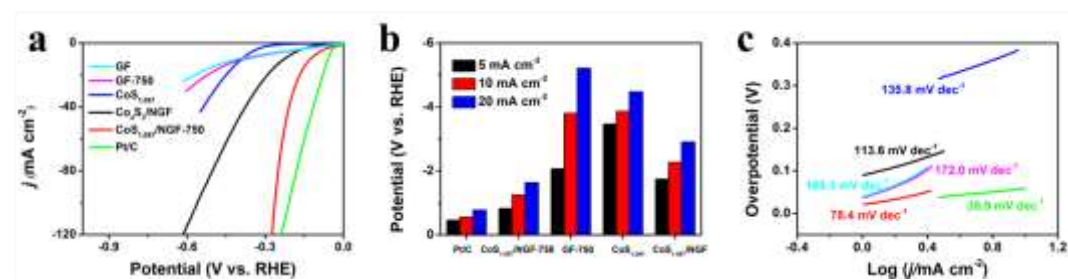
Fig. S12. Electrochemical HER properties of the electrocatalysts in 1 M KOH solution. (a) Polarization curves (iR-corrected) at a scan rate of 5 mV s^{-1}, (b) Potentials corresponding to different current densities (5, 10, 20 mA cm^{-2}) and (c) Tafel plots of GF, GF-750, $CoS_{1.097}$, Co_4S_3/NGF, $CoS_{1.097}$/NGF-750 and Pt/C.

Table S1. Electrochemical properties of $CoS_{1.097}$/NGF-(650~950) materials toward OER in 1 M aqueous KOH solution.

Sample	$CoS_{1.097}$/NGF -650	$CoS_{1.097}$/NGF -750	$CoS_{1.097}$/NGF -850	$CoS_{1.097}$/NGF -950
Rct (Ω)	6.3	1.0	2.4	2.8
Cdl ($mF\ cm^{-2}$)	6.7	82.7	44.4	31.9
ESCA (cm^2)	167.5	2067.5	1110	797.5

Table S2. Comparison of the electrocatalytic activity toward OER for $CoS_{1.097}$/NGF-750 and other recently reported active non-noble metal based catalysts in alkaline solution.

Electrocatalysts	$\eta_j = 10\ mA\ cm^{-2}$ (mV)	Stability Test	Retention Ratio	Electrolyte	Reference
Co_9S_8@NOSC-900	340	10 h	~83%	1 M KOH	S11
P-CoMoS/CC	260	24 h	~91%	1 M KOH	S12
N-Co_9S_8/G	409	-		0.1 M KOH	S13
$Co_{0.5}Fe_{0.5}S$@N-MC	310	20000 s	~98%	1 M KOH	S14
Co/Co_9S_8@SNGS-1000	290	-		0.1 M KOH	S15
NiCoPS/CC	230	40 h	~97%	1 M KOH	S16
$NiCo_2S_4$ NW/NF	260	10 h	~85%	1 M KOH	S17
Co_9S_8@CT-800	390	-		0.1 M KOH	S18
$CoS_{1.097}$/NGF-750	240	40 h	~99%	1 M KOH	This work

Table S3. Comparison of full water splitting performance in alkaline electrolytes for $CoS_{1.097}$/NGF-750 and other recently reported active non-noble metal based electrolyzers.

Electrocatalysts	$\eta_j = 10$ mA cm^{-2} (mV)	Stability Test	Retention Ratio	Electrolyte	Reference
$Ni_xCo_{3-x}S_4/Ni_3S_2$/NF	1.53	200 h	~90 %	1 M KOH	S1
Co_9S_8@NOSC-900	1.60	10 h	~96%	1 M KOH	S11
$NiCo_2S_4$ NW/NF	1.63	50 h	~87%	1 M KOH	S17
Co_9S_8/WS_2	1.65	24 h	~90%	1 M KOH	S19
NS/rGO-Co_4	1.68	-		0.1 M KOH	S20
$CoS_{1.097}$/NGF-750	1.56	45 h	~95%	1 M KOH	This work

Table S4. The correction of zero point energy and entropy of the adsorbed and gaseous

species.

	ZPE(eV)	TS(eV)
*OOH	0.35	0
*O	0.05	0
*OH	0.31	0.01
H_2O	0.56	0.67
H_2	0.27	0.41

References

S1 Y. Wu, Y. Liu, G.-D. Li, X. Zou, X. Lian, D. Wang, L. Sun, T. Asefa, X. Zou, *Nano Energy* 2017, **35**, 161-170.

S2 G. Kresse, J. Furthmüller, *Phys. Rev.* B 1996, **54**, 11169-11186.

S3 G. Kresse, J. Hafner, *Phys. Rev. B* 1994, **49**, 14251-14269.

S4 P. E. Blöchl, *Phys. Rev. B* 1994, **50**, 17953-17979.

S5 J. P. Perdew, K. Burke, M. Ernzerhof, *Phys. Rev. Lett.* 1996, **77**, 3865-3868.

S6 Y. Zhang, W. Yang, *Phys. Rev. Lett.* 1998, **80**, 890-890.

S7 B. Hammer, L. B. Hansen, J. K. Nørskov, *Phys. Rev. B* 1999, **59**, 7413-7421.

S8 H. J. Monkhorst, J. D. Pack, *Phys. Rev. B* 1967, **13**, 5188.

S9 J. K. Nørskov, J. Rossmeisl, A. Logadottir, L. Lindqvist, J. R. Kitchin, T. Bligaard, H. Jonsson, *J. Phys. Chem. B* 2004, **108**, 17886-17892.

S10 J. K. Nørskov, T. Bligaard, A. Logadottir, J. Kitchin, J. G. Chen, S. Pandelov, U. Stimming, *J. Electrochem. Soc.* 2005, **152**, J23-J26.

S11 S. Huang, Y. Meng, S. He, A. Goswami, Q. Wu, J. Li, S. Tong, T. Asefa, M. Wu, *Adv. Funct. Mater.* 2017, **27**, 1606585.

S12 C. Ray, S. C. Lee, K. V. Sankar, B. Jin, J. Lee, J. H. Park, S. C. Jun, *ACS Appl. Mater. Interfaces* 2017, **9**, 37739-37749.

S13 S. Wang, S. Dou, L. Tao, J. Huo, L. Dai, *Energy Environ. Sci.* 2016, **9**, 1320-1326.

S14 M. Shen, C. Ruan, Y. Chen, C. Jiang, K. Ai, L. Lu, *ACS Appl. Mater. Interfaces* 2015, **7**, 1207-1218.

S15 X. Zhang, S. Liu, Y. Zang, R. Liu, G. Liu, G. Wang, Y. Zhang, H. Zhang, H. Zhao, *Nano Energy* 2016, **30**, 93-102.

S16 J. Li, Z. Xia, X. Zhou, Y. Qin, Y. Ma, Y. Qu, *Nano Res.* 2017, **10**, 814-825.

S17 A. Sivanantham, P. Ganesan, S. Shanmugam, *Adv. Funct. Mater.* 2016, **26**, 4661-4672.

S18 T. Liu, L. Zhang, Y. Tian, *J. Mater. Chem. A* 2018, **6**, 5935-5943.

S19 S. Peng, L. Li, J. Zhang, T. L. Tan, T. Zhang, D. Ji, X. Han, F. Cheng, S. Ramakrishna, *J. Mater. Chem. A* 2017, **5**, 23361-23368.

S20 N. Wang, L. Li, D. Zhao, X. Kang, Z. Tang, S. Chen, *Small* 2017, **13**, 1701025.